Journal of Applied Physics

Ion percolation through annealed, supported graphene oxide films: Role of nanochannels and voids

Cite as: J. Appl. Phys. **125**, 144304 (2019); https://doi.org/10.1063/1.5080523
Submitted: 09 November 2018 . Accepted: 23 March 2019 . Published Online: 11 April 2019

Vasumathy Ravishankar, S. Ramaprabhu, and Manu Jaiswal

Journal of Applied Physics ARTICLE scitation.org/journal/jap

Ion percolation through annealed, supported graphene oxide films: Role of nanochannels and voids

Cite as: J. Appl. Phys. **125**, 144304 (2019); doi: 10.1063/1.5080523
Submitted: 9 November 2018 · Accepted: 23 March 2019 ·
Published Online: 11 April 2019

Vasumathy Ravishankar,[1,2] S. Ramaprabhu,[1] and Manu Jaiswal[2,a)]

AFFILIATIONS

[1]Alternative Energy and Nanotechnology Laboratory, Department of Physics, Indian Institute of Technology Madras, Chennai 600036, India
[2]Graphene and 2D Systems Laboratory, Department of Physics, Indian Institute of Technology Madras, Chennai 600036, India

[a)]Author to whom correspondence should be addressed: manu.jaiswal@iitm.ac.in

ABSTRACT

Graphene oxide (GO), an ionic and molecular sieve, is an important material for wide-spectrum filtration, since its properties can be tuned by controlling the structure and dimensions of nanochannels between GO nanosheets. In the literature, mechanisms of ion percolation have been proposed assuming GO to be a uniform structure of vertically stacked graphene sheets decorated with functional groups, termed as lamellae. However, in practice, GO is known to have a hierarchical microstructure. In the present work, supported GO films annealed at different temperatures have been studied with the aim of discerning the relative contributions of nanochannels and voids, gaps between the lamellae, using electro-impedance spectroscopy, and the results were fitted to equivalent circuits. Monotonous decrease in the charge transfer resistance R_{ct} and an increase in the percolation resistance R_P were observed for GO films annealed up to 160 °C. Increase in R_P, taken in perspective with a gradual loss of ordering in nanosheets as observed from X-ray diffraction spectra, enables the conclusion that nanochannels are the dominant pathways of percolation. This was further confirmed by the response of GO films annealed at 180 °C and 200 °C, where a strong dynamic is observed. For these annealed GO films, charge transfer happens both in the conducting films and at the fluorine-doped tin oxide interface. The two processes of ion percolation and charge transfer are, however, interdependent, and are not separated in the impedance response.

I. INTRODUCTION

Intercalated water in graphite oxide has been studied extensively since it was first known, using gravimetry,[1] X-ray diffraction (XRD),[2,3] Fourier transform infrared spectroscopy (FTIR),[3] and neutron diffraction.[4] Studies have also described hydration dynamics in graphite oxide.[5] Post discovery of graphene, studies have offered new perspectives on intercalated water and its role in the physics and chemistry of graphene oxide (GO).[6–10] With the discovery of fast percolation of water and ions across GO films, they have been increasingly studied in both pristine and modified forms as possible filtration membranes.

Water transport through GO films is associated with the sp^2 regions contained within the sp^3 rich matrix. The sp^2 regions provide frictionless flow, while the sp^3 regions serve as spacers that create sufficient width in the nanochannels so that one or few monolayers of water can be accommodated.[11,12] The basic building blocks of GO films are GO nanosheets, sometimes referred to as flakes.[13] These nanosheets consist of domains of purely graphitic and hydrophobic sp^2 hybridized regions, and functionalized hydrophilic sp^3 hybridized regions.[14–16] Consequently, the water intercalated between nanosheets may be classified into two types: "mobile," that is present between hydrophobic regions, and "bound water," that is attached to oxygen containing functional groups through hydrogen bonds.[3,9] The mobile water containing sp^2 regions form a network of pathways that facilitates water percolation,[11,12] and this network is termed as "nanochannels." The spacing between the GO nanosheets is tuneable and its value is between 4 Å and 10 Å depending on the oxidation state of GO. The hierarchical microstructure of GO is observed in samples prepared by different methods: vacuum assisted, dip coated, and drop cast self-assembled films.[17–19] A collection of such neatly

stacked GO nanosheets is termed as "lamellae." Thicker films are a collection of lamellae, separated by features termed as "voids." Figure 1 shows a schematic of this hierarchical microstructure of GO. Though the degree of ordering depends on the method of preparation, a hierarchical structure has been reported for a film thickness greater than 100 nm.[20] Recently, one school of thought has attributed the unusually high water percolation flux to this hierarchical structure, with the flux through voids and gaps dominating the response.[19] They argued that membrane compaction leads to the collapse of these lamellae, resulting in flux reduction.

Ion percolation and water percolation processes are related to each other, since the ions typically move in their hydrated state. The water flux and ion fluxes have been shown to be correlated for GO prepared with different nanochannel widths.[21] In their study, the idea of ion dehydration was proposed for percolation through nanochannels.[22] Simulation shows that partial shedding of hydration shells enables ions to pass through channels that are smaller than their hydrated diameter. Experimental evidence of this was claimed when the nanochannel size was tuned by physically confining GO.[21] However, such an approach is also not capable of distinguishing percolation through nanochannels and percolation between lamellae, i.e., through the voids.

The fundamental reason for the lack of consensus on the mechanism of ion percolation is that the percolation through nanochannels and through voids cannot be directly studied. The approach available is to either tune or eliminate one of the factors, typically the voids. The results depend on the assumptions used, for example, to estimate the pore density from the flake size[13] or estimate the void density from cross-sectional images. The morphology and structure of the film during water and ion percolation may not match the one identified from *ex situ* studies. Importantly, most experiments are performed on suspended films, which tend to bulge to different extents depending on the morphology involved. The bulging can be expected to enhance the role of voids and gaps for the ion percolation. To summarize, an approach is needed which addresses some of the problems associated with suspended films.

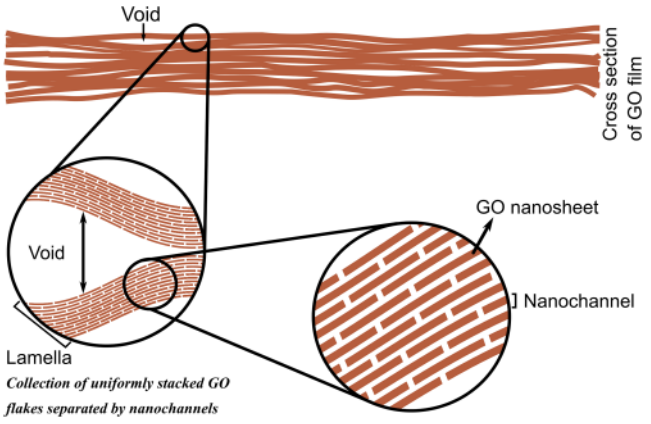

FIG. 1. Schematic of a hierarchical microstructure of GO.

In this work, an attempt has been made to study the relative contributions of nanochannels and voids in the percolation of ions through supported graphene oxide films with an aim to address the open question of whether ion percolation predominantly occurs through nanochannels or voids. Supported GO films were used to eliminate any deformation of the films. An approach relying on electro-impedance spectroscopy (EIS) was adopted. It is an often used tool to study ion percolation in membranes and biological systems.[23–25] Voids being much larger in size than the nanochannels, EIS was expected to have the capability to distinguish percolation at these two length scales. Annealing is a thermal treatment that is known to cause reduction in GO (i.e., oxygen containing functional groups are removed from GO), and it was expected that the hierarchical microstructure of GO, i.e., the nanochannel width and the number of voids, could be tuned through annealing.

We envisage that clarity on the percolation pathways will enable engineering the material effectively, which may be useful for applications in desalination and water filtration. Furthermore, impedance spectroscopy can be used to quickly evaluate the ion percolation state of a GO film based on this work.

II. EXPERIMENTAL

Aqueous GO solution (Graphene Supermarket, 6 mg/ml, >80% monolayer) was used to prepare films on fluorine-doped tin oxide (FTO) (Sigma Aldrich, 7 Ω/sq sheet resistance). The GO films studied in this work using EIS were prepared by spin coating a 3 mg/ml diluted solution of GO in ethanol, on FTO substrates. These films were annealed at six different temperatures, between 100 °C and 200 °C (10 °C/min ramp rate) in a tube furnace (Lindberg Blue) in an inert atmosphere of argon (70 sccm) in multiple batches.

GO films were examined under an optical microscope to verify good contact with the FTO substrate. X-ray diffraction (XRD) was carried out on a Rigaku SmartLab X-ray diffractometer at the Cu K-alpha line. Attenuated total reflection Fourier transform infrared spectroscopy (ATR-FTIR) was conducted in the transmission mode using an Agilent Cary 630 FTIR spectrometer. Cross-sectional scanning electron microscopy (SEM) was performed on as-prepared GO films and on films annealed at 200 °C, made using the drop cast method, with an INSPECT F50 SEM system, at a 30 keV acceleration voltage. Raman spectra were obtained using Horiba LabRAM HR-UV using a He-Ne source at an excitation wavelength of ~633 nm. Impedance spectra were recorded for a total of 21 samples (three samples at six annealing temperatures and three as-prepared samples) using an Ivium Compactstat EIS system. EIS was carried out by applying a sine wave of amplitude 10 mV at frequencies of 10^{-2} Hz to 10^{4} Hz, logarithmically spaced at 6 points per decade for all scans. Equivalent circuits were used to fit the data. All measurements were made in the standard 3-electrode configuration. GO on the FTO substrate was used as the working electrode (WE), a platinum wire was used as the counter electrode (CE), and Ag/AgCl acted as the reference electrode (RE). A potassium chloride (KCl) solution of 0.1M concentration was used as the electrolyte. A custom-made polytetrafluoroethylene (PTFE) device was used as the cell.

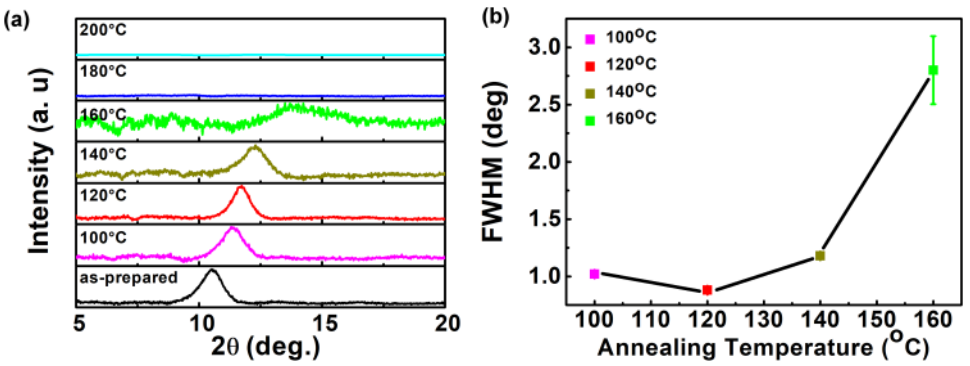

FIG. 2. (a) XRD spectra: XRD peak around 10°, corresponding to the (001) plane of GO, shifts rightward with increasing annealing temperatures. The peak is not resolved for annealing temperatures above 180 °C. (b) Full width at half maximum vs annealing temperature. The black line is a guide to the eye.

For EIS studies, eight scans of spectra were recorded over a duration of ∼60 min, after which no change in the spectrum was noted; this was taken to be the steady state. Films supported on FTO were used; to minimize any transmembrane pressure, the films fabricated were typically 500 nm in thickness. FTO also served the purpose of being an electrode.

III. RESULTS AND DISCUSSION

Figure 2(a) shows X-ray diffraction spectroscopy of as-prepared GO and GO annealed from 100 °C to 200 °C. One peak at ∼10.5° corresponding to the (001) plane was obtained for as-prepared GO films. Between annealing temperatures of 100 °C and 160 °C, this peak shifted to higher 2θ values. For annealing temperatures of 180 °C and 200 °C, this peak was not resolved. The absence of a clear peak should be seen in the context of the increasing broadening of the XRD peak seen from 100 °C to 160 °C. Further increase in the microstructural disorder made the broadened peak signal comparable to the noise level of measurement. The position of the (001) peak was dependent on the presence of a functional group as well as intercalated water, indicating that the shift of this peak may be due to the loss of both water and the functional group with annealing temperature.[26–28] The average nanochannel width decreased with annealing temperature,[7] and the values obtained in this study are shown in Table I. The vanishing of the peak may be attributed to a loss of long-range ordering in the system. FWHM increased abruptly from 1.18 to 2.8 as annealing temperature was changed from 140 °C to 160 °C. This is indicative of an increase in the microstructural disorder and a decrease in the crystallite size, and is consistent with other reports.[29] Further, the Scherrer formula[30] was used to estimate the average number of ordered layers in a single crystallite along the (001) direction, and it was found to change from 12 layers for GO annealed at 120 °C to 9 for GO annealed at 140 °C and to only 5 for GO annealed at 160 °C. It has been discussed in a previous report that the estimates made from the Scherrer formula for annealed GO films are broadly consistent with those made from more refined approaches.[29]

Figure 3 shows the SEM images of an as-prepared GO film and that annealed at 200 °C. For the as-prepared GO film, the number of voids is very few, while for the annealed GO film, the number of voids increases, corroborating the microstructural disorder noted in XRD results.

TABLE I. Nanochannel width vs annealing temperature, obtained from X-ray diffraction (XRD) studies.

Annealing temperature (°C)	2Θ peak position for (001) peak (deg)	Nanochannel width (Å)
As-prepared	10.49	8.4
100	11.33	7.8
120	11.70	7.6
140	12.26	7.2
160	14.22	6.2
180	…	…
200	…	…

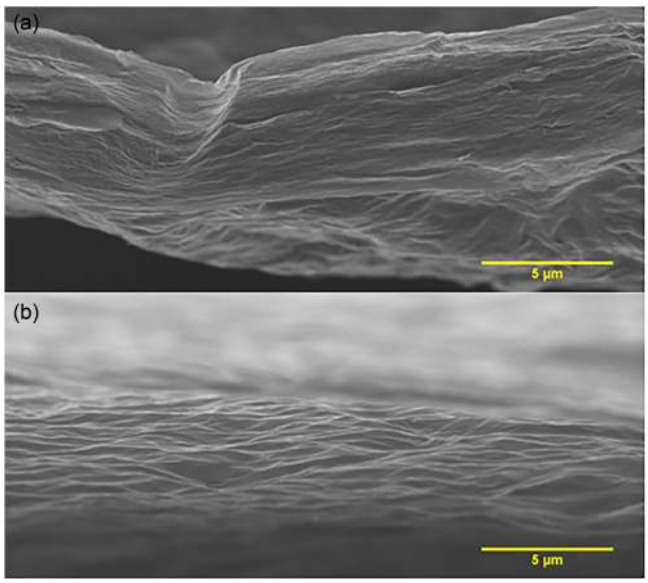

FIG. 3. Cross-sectional scanning electron microscopy images: (a) an as-prepared GO film and (b) a GO film annealed at 200 °C.

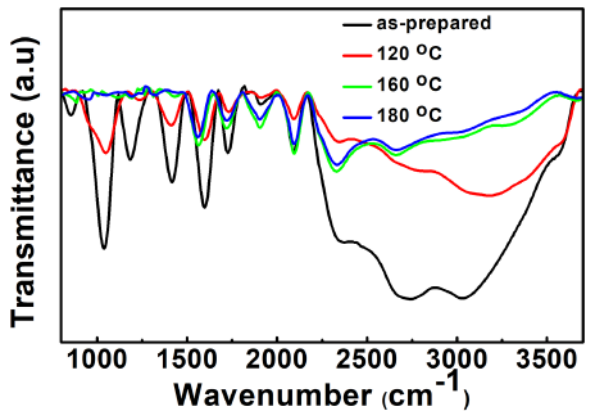

FIG. 4. ATR-FTIR spectrum of as-prepared and annealed GO. The broad peak between 2400 cm^{-1} and 3700 cm^{-1} decreases in intensity as the annealing temperature increases.

Figure 4 shows the FTIR spectrum for as-prepared and annealed GO films. Spectra were taken between 800 cm^{-1} and 3700 cm^{-1}. Broadly, the spectrum may be classified into three regions: the fingerprint region below 1500 cm^{-1}, two characteristic peaks, 1602 cm^{-1} and 1725 cm^{-1}, lying in the middle of the spectrum, and the broad peak between 2400 cm^{-1} and 3700 cm^{-1}.[20] Between 900 cm^{-1} and 1100 cm^{-1}, the modes correspond to ether derivatives. Between 1100 cm^{-1} and 1280 cm^{-1}, the modes correspond to ketonic species. Between 1280 cm^{-1} and 1500 cm^{-1}, the modes correspond to epoxides.[26,31] The 1602 cm^{-1} mode corresponds to the bending modes of water in the GO. The 1725 cm^{-1} band is attributed to the stretching modes of the carbonyl group. The broad peak between 2400 cm^{-1} and 3700 cm^{-1} in the FTIR spectrum is attributed to the stretching modes of –OH with major contributions from confined water.[32] This peak decreases in intensity as annealing temperature increases. For an annealing temperature of 180°C, all confined water is expelled from the GO layers, resulting in a sharp decrease in intensity between 3000 cm^{-1} and 3700 cm^{-1}. Thus, at higher annealing temperatures, the loss of both functional groups and intercalated water occurs. We note that FTIR reveals the presence of GO, albeit without confined water, at 180 °C, even as the microstructurally disordered GO shows no clear XRD peak.

From the above studies, it can be inferred that with annealing, the number of voids increases, while the nanochannel width decreases. Therefore, annealing has the dual effect of increasing the number of voids due to a disordered microstructure and decreasing the nanochannel width.

Presented in Fig. 5(a) is the impedance response of DI water with FTO as the working electrode in the frequency range 10^{-2} Hz to 10^{4} Hz. The data were taken in the same setup as for GO films. Presented in Fig. 5(b) is the impedance response of DI water using a GO-coated FTO.

We next discuss the EIS response of the annealed GO films. Figure 6(a) shows the impedance response of a bare FTO substrate. Inset shows the equivalent circuit used to fit the response. R_S is the solution resistance, R_{ct} is the charge resistance, and C_{dl} is the double layer capacitance at the FTO–electrolyte interface. The electrode in an electrolyte gives rise to a charge double layer at the interface of the electrolyte and the conductor, which can be modulated using an external voltage.[33] The charge double layer can be modeled as a capacitor (C_{dl}). In most real systems, the double layer allows electrical charges to be exchanged between the electrode and the electrolyte. The resistance that is offered to this transfer of electrons is termed charge transfer resistance R_{ct}. The value of R_{ct} depends on the nature of the interface and the area of the interface. For FTO, a single broad peak is seen in the spectrum which corresponds to the charge transfer resistance—R_{ct} is of the order of $M\Omega/mm^2$ (see Table II) and thus a slow charge transfer process.

Figures 6(b)–6(h) show representative Bode plots for as-prepared and annealed GO films. The responses displayed have not been normalized to area. Figures 6(i) and 6(j) show circuit models used for fitting the response. The response for an as-prepared GO film is shown in Fig. 6(b). Two peaks are observed—the peak at a higher frequency was attributed to percolation because of the relatively quick dynamics of hydration in liquid water.[11,12] The circuit shown in Fig. 6(i) was used to fit the response of as-prepared GO films and those annealed up to 160 °C. The circuit consists of two RC elements in series with the solution resistance R_S. Q_P is the constant phase element (CPE) associated with nanochannel walls, R_P is

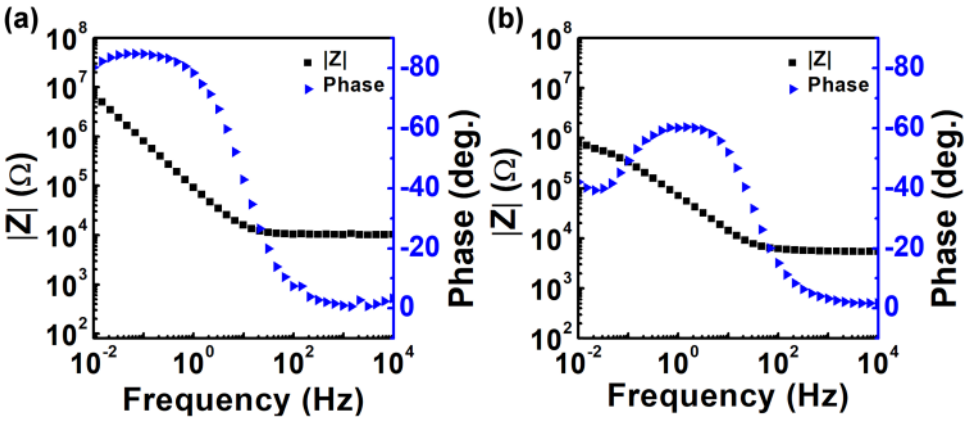

FIG. 5. (a) Impedance response of DI water and (b) impedance response of GO with DI water.

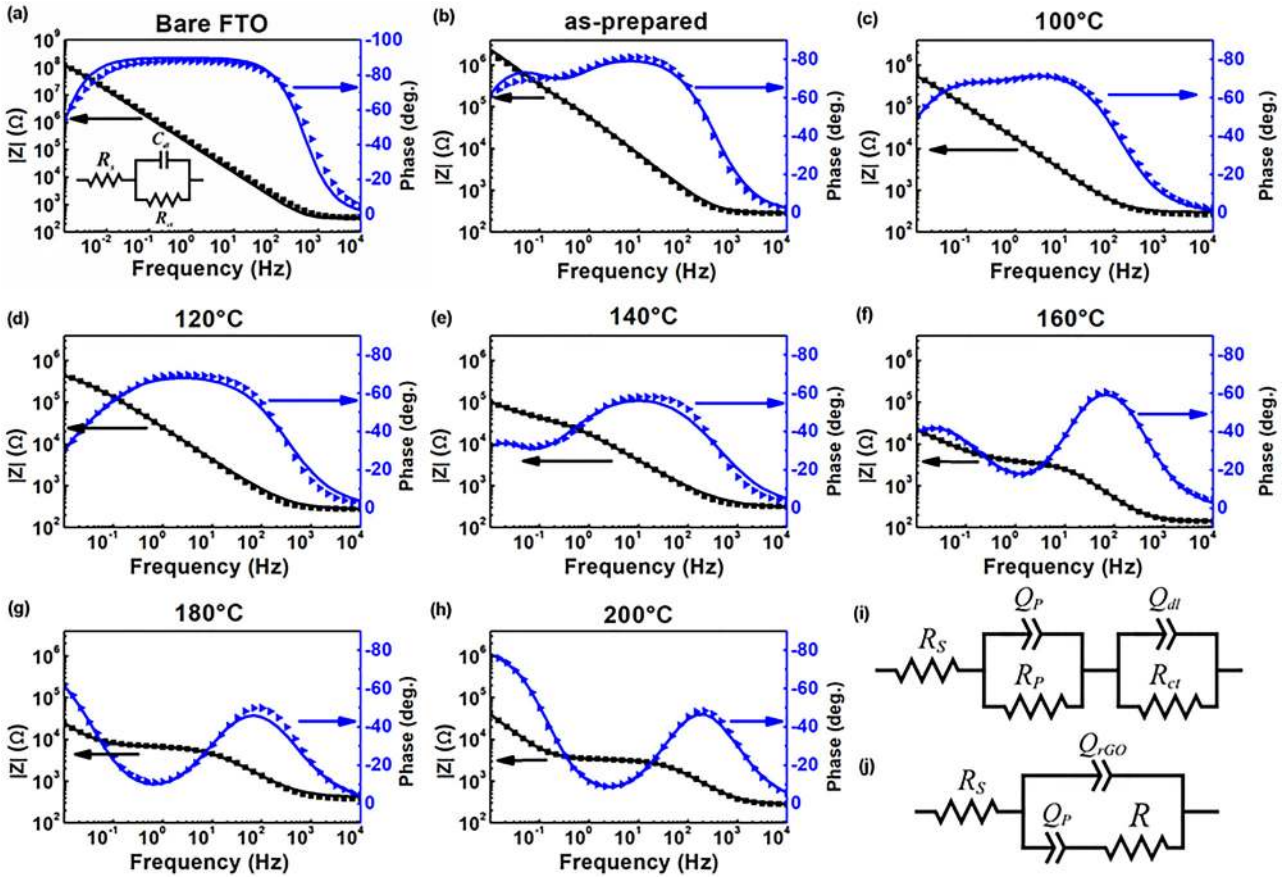

FIG. 6. (a) Impedance response of FTO. The points indicate experimental values and the solid line indicates fit. The inset shows the equivalent circuit used to fit this response. Impedance response of (b) an as-prepared GO (c) a GO annealed at 100 °C (d) 120 °C (e) 140 °C, (f) 160 °C, (g) 180 °C, and (h) 200 °C. (i) An equivalent circuit for the as-prepared GO and the GO annealed up to 160 °C. (j) The equivalent circuit for the GO annealed at and above 180 °C.

the resistance offered by the film for the movement of ions through the percolating network of sp^2 hybridized pathways, Q_{dl} is the CPE associated with the electrolyte and the FTO substrate interface, and R_{ct} is the charge transfer resistance. CPE may be defined as an imperfect capacitor, whose impedance Z_{CPE} is given by

$$Z_{CPE} = \frac{1}{(i\,\omega)^n Q},$$

where n is the exponent whose value lies between 0 and 1. If the value is 1, it corresponds to an ideal capacitor, and if the value is 0, it corresponds to an ideal resistor. Note that Q does not have the dimensions of capacitance. For the as-prepared film, a small percolation resistance, of the order of 100 Ω is observed. Peak at a lower frequency corresponds to the charge transfer process. It is to be noted that the charge transfer resistance is two orders of magnitude lesser for the FTO–GO system than the bare FTO substrate. In the GO system, there are two kinds of interfaces: an electrolyte with the sp^2 hybridized region in GO (which are the conducting regions) and an electrolyte with FTO. At both these interfaces, a charge double layer is formed, resulting in a transfer of electrons. Thus, the additional charge transfer pathways in the form of sp^2-rich regions of GO are the likely explanation for this reduction in R_{ct}. From Figs. 5 and 6(b), it is clear that the impedance responses of GO in contact with the KCl electrolyte arise from the percolation of ions in GO.

TABLE II. Fit parameters for a bare FTO. The EIS response was fit according to the circuit shown in the inset of Fig. 6(a).

R_s (Ω)	R_{ct} (MΩ/mm^2)	C_{dl} (nF/mm^2)
326.7	2.62	0.13

Figures 6(c)–6(e) show the response of GO between 100 °C and 140 °C. Here, two peaks can still be seen; however, the separation between the two is less distinct than for the as-prepared GO film. Figure 6(f) shows the impedance response of GO at 160 °C. Though the response seems to have a single peak, it was possible to resolve the R_{ct} and R_P by the fits. Figures 6(g) and 6(h) show the

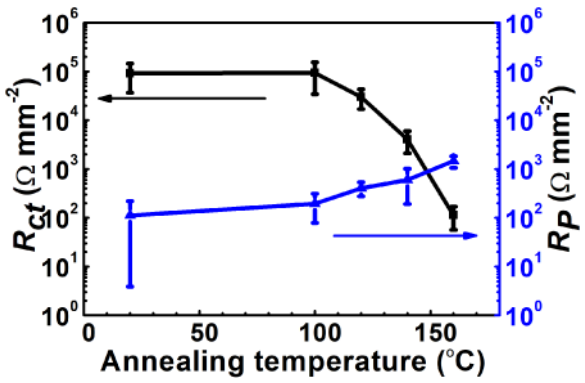

FIG. 7. Variation of area normalized R_P and R_{ct} as a function of annealing temperature for as-prepared GO films and GO films annealed upto 160 °C.

frequency response of GO films annealed at 180 °C and 200 °C. A single prominent peak is observed at these temperatures. The circuit shown in Fig. 6(j) was used to fit the response at these annealing temperatures. R_S is the solution resistance, Q_{rGO} is the CPE associated with the bulk film, Q_P is the CPE associated with the charge double layer at the nanochannels, and R is the combination of R_P and R_{ct}. At lower annealing temperatures, the charge transfer mainly happens at the FTO interface. At higher annealing temperatures, sp^2 regions of annealed GO (rGO) itself serve as a platform for charge transfer. Thus, percolation and charge transfer are no longer spatially distinct processes, but are rather interdependent. Therefore, it was not possible to resolve R_{ct} and R_P as separate circuit elements, likely because charge transfer is determined by the percolation of ions into the GO layers.

The fit values of R_{ct} and R_P are shown in Fig. 7; the values displayed have been normalized to the area exposed to measurement. A steady decrease is seen in R_{ct} between the as-prepared GO and the GO annealed at 160 °C. Also, R_P increases with an increase in annealing temperature. The decrease in R_{ct} can be attributed to increasing sp^2 regions due to the loss of functional groups with annealing. R_{ct} being the charge transfer resistance between the electrolyte and FTO as well as sp^2 hybridized regions in GO, increasing sp^2 islands dominate charge transfer.

The increase in sp^2 regions may be understood from examining the I_D/I_G ratio from Raman spectroscopy shown in Fig. 8. A representative Raman spectrum is shown in Fig. 8(a) for graphene oxide annealed at 160 °C. One of the main modes, seen at 1592 cm^{-1}, is the G peak due to the in-plane vibration of optical phonons of pristine graphene lattice around the Γ point. The defect peak, otherwise known as the D peak at 1334 cm^{-1}, is an intravalley scattering process around the K point, and is mainly due to the oxygen rich functional groups. A faint 2D peak, arising from a two-phonon, intravalley scattering process around the K point is seen around 2646 cm^{-1}.[34] A monotonic increase in the ratio of the area integrated intensities of the D peak to the G peak is seen in Fig. 8(b) and indicates a gradual loss of functional groups, resulting in larger sp^2 hybridized regions.[31,35,36] As for the increase in R_P, the loss of functional groups, shown in FTIR (Fig. 4), results in a decrease of the average nanochannel width, shown by XRD (Table I). Thus, there is more resistance to ion percolation due to the decrease in width of the nanochannels.

The decrease in R_P is due to the decrease in the nanochannel width with increasing annealing temperature. Figure 9 shows the variation of R_P for first scan, with the average nanochannel width obtained from XRD. R_P has an exponential dependence on the nanochannel width and was fit using the empirical formula,

$$R_P(d) = R_0 e^{-\lambda d},$$

where d is the nanochannel width, $R_0 \approx 0.9$ MΩ/mm^2 from the fit to the data in Fig. 9, and $\lambda \approx 1.0$ Å^{-1}. R_P asymptotically meets zero at a large interwall separation.

Also recall that there is an increase in FWHM of the (001) XRD peak for increasing annealing temperatures and thus an increase in the number of voids in the GO film as annealing temperature increases. Despite this, the overall percolation resistance R_P increases upon annealing. We therefore suggest that, between nanochannels and voids, the former is the dominant factor for ion percolation in the supported GO.

We next discuss the time dependence of the frequency response for these supported films. Figure 10 shows the dynamics for films annealed at 160 °C, and the responses have not been normalized to area. No change in response was observed for consecutive scans for these films—each scan lasted a period of 8 min, and the total duration of the experiment was 60 min. This could be due

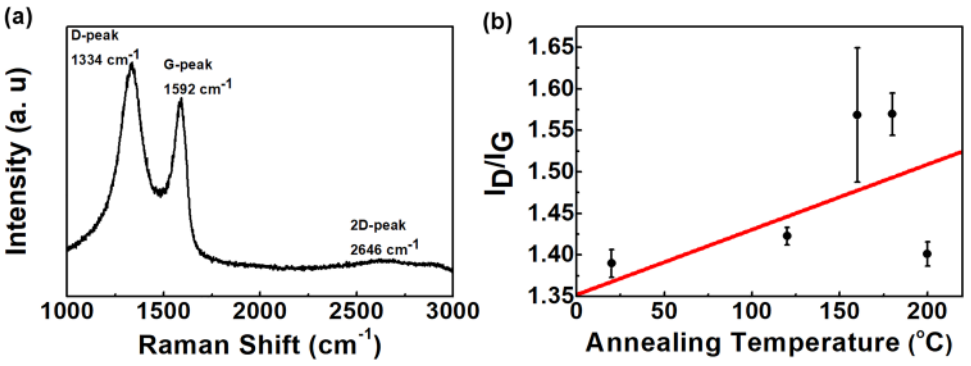

FIG. 8. Raman spectrum. (a) A typical Raman spectrum of graphene oxide. (b) Increasing I_D/I_G ratio with annealing temperature, showing an increase in sp^2 islands in graphene oxide.

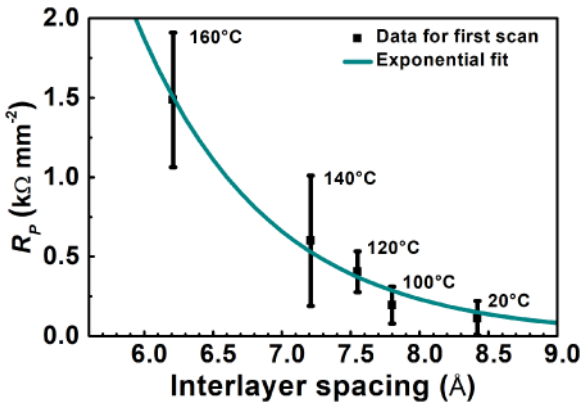

FIG. 9. Exponential fit for R_P of first scan as a function of the nanochannel width for annealing temperatures up to 160 °C. The annealing temperature is shown as labels to data points.

to the fact that the dynamics was quick, and, could not be captured in the duration of one scan, and these measurements may be thought of as being made at steady state. A similar response was seen in GO films annealed at lower temperatures and in as-prepared GOs. Graphene oxide is known to swell in water, meaning, water intercalates between the nanosheets, resulting in an increase in the nanochannel width. In liquid water, the nanochannel width can increase up to 13 Å for a GO that has not been annealed.[21] In this study, there is no marked change in the values of R_P over the period of study (~60 min). Hence, there is no significant swelling of GO within this time period.

We next look at the dynamics for films annealed at higher temperatures ($T \geq 180$ °C). Figure 11 shows the time-dependent response for one film annealed at 200 °C, values not normalized to area. The low frequency magnitude, as well as the peak position in the phase plots, changes with every scan. For each scan, a suitable circuit can be fit, in principle. However, one must bear in mind that the values of these elements were observed to drift during the interval of the scan, and thus, the values must be considered as average values over the period of the scan.

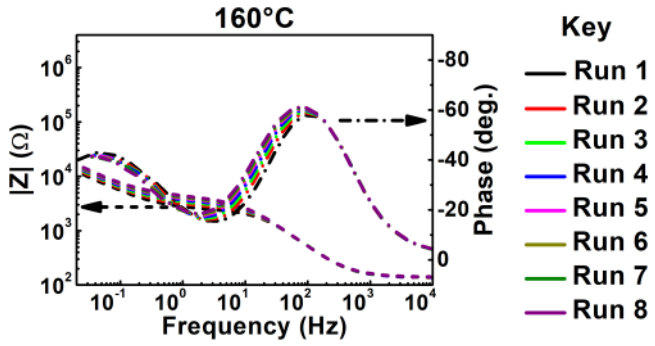

FIG. 10. Time-dependent response of a GO film annealed at 160 °C.

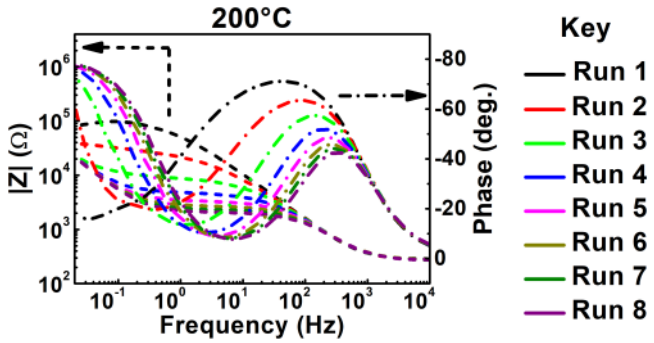

FIG. 11. Time-dependent response of a GO film annealed at 200 °C.

The question then is, why do GO films annealed at higher temperatures show large dynamics? We have already reconciled to the different nature of equivalent circuit for films annealed at and above 180 °C: the percolation process and the charge transfer process are no longer independent processes in series but appear as a "combined circuit element." Ions permeate the GO nanochannels gradually, because, in films annealed at higher temperatures, there is considerable resistance to ion movement. The percolation brings in a more effective area of rGO in contact with ions; thus, charge transfer can occur only as percolation progresses. As more areas of sp^2 hybridized GO comes in contact with the electrolyte, the charge transfer resistance decreases. The dynamics is representative of this interdependence of percolation and charge transfer.

Recall that rGO has a large microstructural disorder at and above 160 °C annealing, as verified by XRD studies. The voids in a microstructurally disordered GO continue to offer quick pathways to ions, to the FTO interface. However, steady state is not reached for a period of ~60 min (corresponding to 8 scans). Thus, we see once more that nanochannels may be playing a more important role than voids in the ion percolation process.

Since percolation and charge transfer are coupled in these films, the contribution to impedance from both Q_P and R was examined, at the lowest applied frequency 10 mHz. Q_{rGO} being two orders of magnitude smaller than Q_P, that element may be treated as open at 10 mHz, and the low frequency contribution is mainly from the $Q_{P\text{-}R}$ branch. This is the case for both 180 °C and 200 °C annealing temperatures. The different components of the total impedance $Z_{QP\text{-}R}$ were plotted as a function of time. Data shown here are for three films annealed at 200 °C. Figure 12(a) shows the variation of modulus of impedance due to Q_P, $|Z_{QP}|$, and R, respectively. It can be seen that both parameters have an exponential variation with time. The major contribution to impedance comes from double layer charging at the nanochannel walls. Further, it can also be noticed from Fig. 11 that the peak moves toward higher frequencies as the dynamics progresses.

The time constant, τ, was calculated for these films. The time constant is given by $\tau = R\,C$, where R is the resistance value obtained from the equivalent circuit fit and C is the capacitance extracted from the Q value of the equivalent circuit fit.

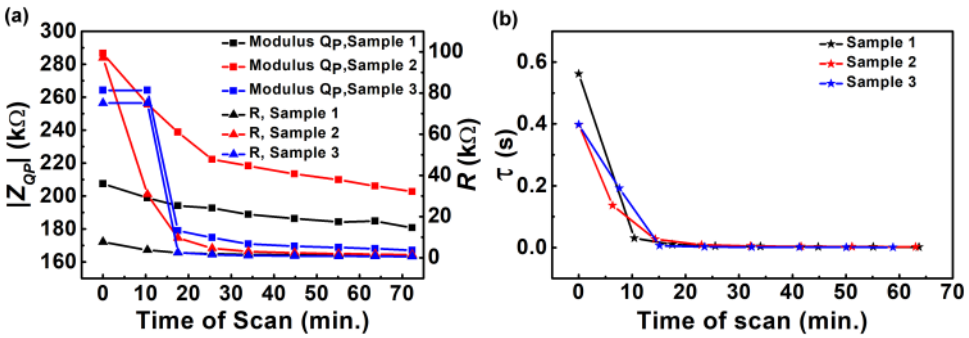

FIG. 12. (a) Variation of impedance due to Q_P and resistance R as a function of scan time. (b) Variation of time constant τ as a function of scan time.

The use of the constant phase element for the fits requires the additional step of calculating capacitance in order to determine τ. This is because, firstly, Q does not have the dimension of farad (F). Secondly, simply using Q instead of C might result in erroneous values of τ. In order to do this, the Hsu–Mansfield[37] approach was employed. This is a suitable approach for nested equivalent circuits like the one used for GO films annealed at 180 °C and 200 °C. The value of capacitance C was obtained using the following formula:

$$C = Q\omega_m{}^{n-1},$$

where Q is the value of the CPE obtained from the equivalent circuit fit, n is the exponent on CPE, and ω_m is the frequency at which Z_{imag} for the response attains a peak. This approach has been explained further in the supplementary material.

Figure 12(b) shows the variation of the time constant (τ) for three films annealed at 200 °C, with the time of measurement. This may be interpreted as faster percolation, probably arising, once again, due to both nanochannels and voids. However, the presence of dynamics confirms the dominant contribution of nanochannels to ion percolation, despite the increase in the microstructural disorder, and thus a decrease in long range ordering of GO nanosheets. If voids were the dominant contribution, dynamics would be absent at these temperatures, due to quick percolation through larger voids.

IV. CONCLUSION

Ion percolation has been studied across graphene oxide films in previous literature. The nanochannel width and the number of voids can be tuned thermally by annealing. It was found in this study that higher annealing temperatures cause a decrease in the nanochannel width and an increase in the number of voids. There has been a lack of consensus on the relative contributions of the network of nanochannels in GO that rapidly conduct water and ions and percolation through voids in the GO film arising due to a hierarchical microstructure. This question was studied using frequency-dependent impedance spectroscopy on GO films with electrically conducting support, and the response was modeled using equivalent circuits. The circuit elements were interpreted as charge transfer resistance and percolation resistance and a strong interplay between them was revealed. The two processes are sequential in as-prepared and GO annealed at relatively lower temperatures, while they are inseparable for GO annealed at higher temperatures. The percolation resistance increases for GO annealed at higher temperatures, even as the microstructural disorder increases and the nanochannel width decreases. While ion percolation through both voids and nanochannels may take place, the role of nanochannels was found to be more important in the ion percolation process.

SUPPLEMENTARY MATERIAL

The supplementary material includes a detailed explanation of the Hsu–Mansfield approach to calculating capacitance and simulated graphs of complex impedance plots and Bode plots to demonstrate the independence of ω_m on exponent n.

ACKNOWLEDGMENTS

M.J. thanks IC&SR, IIT Madras for financial assistance.

REFERENCES

[1]J. L. Gonzales, A. M. Rodrigez, and F. D. Vega, Carbon **7**, 719 (1969).
[2]A. Hamwi and V. Marchand, J. Phys. Chem. Solids **57**, 867 (1996).
[3]S. Cerveny, F. Barroso-Bujans, Á. Alegría, and J. Colmenero, J. Phys. Chem. C **114**, 2604 (2010).
[4]A. Buchsteiner, A. Lerf, and J. Pieper, J. Phys. Chem. B **110**, 22328 (2006).
[5]A. Lerf, A. Buchsteiner, J. Pieper, S. Schöttl, I. Dekany, T. Szabo, and H. P. Boehm, J. Phys. Chem. Solids **67**, 1106 (2006).
[6]B. Rezania, N. Severin, A. V. Talyzin, and J. P. Rabe, Nano Lett. **14**, 3993 (2014).
[7]M. Ghosh, L. Pradipkanti, V. Rai, D. K. Satapathy, P. Vayalamkuzhi, and M. Jaiswal, Appl. Phys. Lett. **106**, 241902 (2015).
[8]W. Guo, J. Chen, S. Sun, and Q. Zhou, J. Phys. Chem. C **120**, 7451 (2016).
[9]R. Wang, H. Gao, D. Zhu, T. Yang, X. Zhang, L. Li, G. Yin, L. Zhu, Z. Feng, and X. Li, Carbon **114**, 23 (2017).
[10]S. Papamatthaiou, D.-P. Argyropoulos, A. Masurkar, M. R. Cavallari, F. Farmakis, I. Kymissis, and N. Georgoulas, Appl. Phys. Lett. **110**, 252106 (2017).
[11]R. R. Nair, H. A. Wu, P. N. Jayaram, I. V. Grigorieva, and A. K. Geim, Science **335**, 442 (2012).
[12]R. K. Joshi, P. Carbone, F. C. Wang, V. G. Kravets, Y. Su, I. V. Grigorieva, H. A. Wu, A. K. Geim, and R. R. Nair, Science **343**, 752 (2014).
[13]V. Saraswat, R. M. Jacobberger, J. S. Ostrander, C. L. Hummell, A. J. Way, J. Wang, M. T. Zanni, and M. S. Arnold, ACS Nano **12**, 7855 (2018).
[14]A. Lerf, H. He, M. Forster, and J. Klinowski, J. Phys. Chem. B **102**, 4477 (1998).
[15]K. Erickson, R. Erni, Z. Lee, N. Alem, W. Gannett, and A. Zettl, Adv. Mater. **22**, 4467 (2010).

[16]C. Gómez-Navarro, J. C. Meyer, R. S. Sundaram, A. Chuvilin, S. Kurasch, M. Burghard, K. Kern, and U. Kaiser, Nano Lett. **10**, 1144 (2010).
[17]K. Nandy, M. J. Palmeri, C. M. Burke, Z. An, S. T. Nguyen, K. W. Putz, and L. C. Brinson, Adv. Mater. Interfaces **3**, 1 (2016).
[18]C. D. Wood, M. J. Palmeri, K. W. Putz, Z. An, S. T. Nguyen, and L. Catherine Brinson, J. Appl. Mech. **80**, 040913 (2013).
[19]J. Y. Chong, B. Wang, C. Mattevi, and K. Li, J. Memb. Sci. **549**, 385 (2018).
[20]A. V. Naumov, *Graphene Oxide: Fundamentals and Applications* (Wiley, Chichester, UK, 2017).
[21]J. Abraham, K. S. Vasu, C. D. Williams, K. Gopinadhan, Y. Su, C. T. Cherian, J. Dix, E. Prestat, S. J. Haigh, I. V. Grigorieva, P. Carbone, A. K. Geim, and R. R. Nair, Nat. Nano **12**, 546 (2017).
[22]S. Sahu, M. Di Ventra, and M. Zwolak, Nano Lett. **17**, 4719 (2017).
[23]C. Steinem, A. Janshoff, H.-J. Galla, and M. Sieber, Bioelectrochem. Bioenerg. **42**, 213 (1997).
[24]I. K. Vockenroth, D. Fine, A. Dodobalapur, A. T. A. Jenkins, and I. Köper, Electrochem. Commun. **10**, 323 (2008).
[25]G. Valincius, M. Mickevicius, T. Penkauskas, and M. Jankunec, Electrochim. Acta **222**, 904 (2016).
[26]M. Acik, C. Mattevi, C. Gong, G. Lee, K. Cho, M. Chhowalla, and Y. J. Chabal, ACS Nano **4**, 5861 (2010).
[27]M. Acik, G. Lee, C. Mattevi, A. Pirkle, R. M. Wallace, M. Chhowalla, K. Cho, and Y. Chabal, J. Phys. Chem. C **115**, 19761 (2011).
[28]K. S. Andrikopoulos, G. Bounos, D. Tasis, L. Sygellou, V. Drakopoulos, and G. A. Voyiatzis, Adv. Mater. Interfaces **1**, 1400250 (2014).
[29]T. M. Pranav, T. Sakorikar, P. Vayalamkuzhi, and M. Jaiswal, J. Appl. Phys. **125**, 24303 (2019).
[30]P. Scherrer, "Nachrichten von Der Gesellschaft Der Wissenschaften Zu Gottingen," Math. Phys. Klasse **2**, 98 (1918) (in German).
[31]V. Rai, M.K. Kavitha, and M. Jaiswal, in *Proceedings of 2015 IEEE International Symposium on Nanoelectronic and Information Systems INIS 2015* (IEEE, 2016), p. 164.
[32]T. Szabó, O. Berkesi, and I. Dékány, Carbon **43**, 3186 (2005).
[33]A. J. Bard and L. R. Faulkner, *Electrochemical Methods Fundamentals and Applications*, 2nd ed. (Wiley, New York, 2000).
[34]L. M. Malard, M. A. Pimenta, G. Dresselhaus, and M. S. Dresselhaus, Phys. Rep. **473**, 51 (2009).
[35]F. Tuinstra and J. L. Koenig, J. Chem. Phys. **53**, 1126 (1970).
[36]L. G. Cançado, A. Jorio, E. H. M. Ferreira, F. Stavale, C. A. Achete, R. B. Capaz, M. V. O. Moutinho, A. Lombardo, T. S. Kulmala, and A. C. Ferrari, Nano Lett. **11**, 3190 (2011).
[37]C. H. Hsu and F. Mansfield, Corrosion **57**, 747 (2001).